Materials Today Bio 19 (2023) 100554

Contents lists available at ScienceDirect

Materials Today Bio

journal homepage: www.journals.elsevier.com/materials-today-bio

Engineered human liver based on pullulan-dextran hydrogel promotes mice survival after liver failure

Camille Le Guilcher [a,*], Grégory Merlen [b], Alessandra Dellaquila [a], Marie-Noëlle Labour [a,c,d], Rachida Aid [a], Thierry Tordjmann [b], Didier Letourneur [a,1,**], Teresa Simon-Yarza [a,1,***]

[a] Université Paris Cité and Université Sorbonne Paris Nord, INSERM, LVTS, U1148, F-75018 Paris, France
[b] Université Paris-Saclay, INSERM U1193, F- 94800 Villejuif, France
[c] ICGM, Université de Montpellier, CNRS, ENSCM, F- 34293 Montpellier, France
[d] École Pratique des Hautes Études, Université Paris Sciences et Lettres, F-75014 Paris, France

ARTICLE INFO

Keywords:
Tissue engineering
3D scaffold
Hepatocyte
Liver failure
Transplantation

ABSTRACT

Liver tissue engineering approaches aim to support drug testing, assistance devices, or transplantation. However, their suitability for clinical application remains unsatisfactory. Herein, we demonstrate the beneficial and biocompatible use of porous pullulan-dextran hydrogel for the self-assembly of hepatocytes and biliary-like cells into functional 3D microtissues. Using HepaRG cells, we obtained 21 days maintenance of engineered liver polarity, functional detoxification and excretion systems, as well as glycogen storage in hydrogel. Implantation on two liver lobes in mice of hydrogels containing 3800 HepaRG 3D structures of 100 μm in diameter, indicated successful engraftment and no signs of liver toxicity after one month. Finally, after acetaminophen-induced liver failure, when mice were transplanted with engineered livers on left lobe and peritoneal cavity, the survival rate at 7 days significantly increased by 31.8% compared with mice without cell therapy. These findings support the clinical potential of pullulan-dextran hydrogel for liver failure management.

1. Introduction

Despite the huge regenerative properties of liver, acute liver failure (ALF) is associated in humans to a mortality rate approaching 70%. A broad range of conditions can severely compromise liver function such as hepatitis or drug-induced liver injury [1]. Shortage of donors for transplantation, treatment insufficiency, and lack of knowledge about the underlying pathologies have encouraged the development of liver tissue engineering (LTE) therapeutic strategies in the last decade [2].

LTE aims to construct three-dimensional (3D) liver tissues as an alternative to two-dimensional (2D) hepatocytes culture models that do not mimic complex tissue structures and exhibit poor long-term viability or functionality' [2,3]. Functional 3D constructs can serve as a testing platform for xenobiotics, as *in vitro* disease models [2,4], as temporary assistance in bioartificial liver devices, or as an alternative for donor organs [2,4,5]. Despite decades of development of technologies, successfully generated 3D liver functional constructs for regenerative medicine still remain a challenge.

In vivo implantation requires biocompatible 3D constructs with an adequate cell source, highly functional, with a well-organized structure, that could be transplanted with an efficient mass sample to maintain liver-specific functions [2,6], easy to handle and to immobilize during transplantation [2–5].

Hepatocytes constitute over two-thirds of liver mass and ensure most of liver functions such as protein synthesis, detoxication and metabolism. However, the limited availability of primary human hepatocytes and their loss of hepatic functions *in vitro* have restricted their use in LTE. The human HepaRG bipotent cell line retains hepatic progenitor-like characteristics and differentiates into hepatocytes and cholangiocytes and partially demonstrates physiological functions similar to mature human hepatocytes when cultivated in the presence of dimethylsulfoxide (DMSO) [7,8]. As many cell types and lines, HepaRG cells display improved hepatocyte functions in 3D compared to 2D culture conditions [9,10]. Besides, free self-assembled hepatocyte spheroids are difficult to

* Corresponding author.
** Corresponding author.
*** Corresponding author.
E-mail addresses: camille.le.guilcher@gmail.com (C. Le Guilcher), didier.letourneur@inserm.fr (D. Letourneur), teresa.simon-yarza@inserm.fr (T. Simon-Yarza).
[1] TSY and DL contributed equally to this study.

https://doi.org/10.1016/j.mtbio.2023.100554
Received 21 September 2022; Received in revised form 15 January 2023; Accepted 17 January 2023
Available online 19 January 2023

obtain in large number and to manipulate, and do not allow control of size or biomechanical microenvironment, precluding their use in liver studies. Therefore, the use of biomaterial scaffolds represents a promising strategy to provide a structural support for 3D differentiation of hepatocytes, and to facilitate their culture, handling and maintenance. However, viability, differentiation and functional ability of HepaRG cells differ between culture methods, size and type of 3D construct [11–15].

There is a large body of studies supporting the use of hydrogels for the production of functional liver 3D constructs thanks to their high content of water and viscoelasticity similar to healthy liver [5,16–18]. Hydrogels prepared with natural polymers have demonstrated good biocompatibility and biodegradability properties compared to most synthetic scaffolds [5,16–18]. However, animal-derived materials use is limited by source availability and variability, low mechanical properties, and high cost. Non animal-derived natural materials are promising systems but none of them currently meet all clinical needs, such as reproducibility of batch, ease to manipulate, or that can be clinically approved [5,16–18]. Moreover, their ability to support *in vivo* liver function and their integration remain poorly characterized.

In this work, we selected pullulan and dextran, two natural polysaccharides used in the pharmaceutical industry. Pullulan is produced from starch fermentation by the fungus *Aureobasidium pullulan*, whose linear polymeric structure offers flexibility. Dextran, synthesized from sucrose by bacteria, provides structural stability thanks to its high molecular weight. The pullulan and dextran combination produces a soft viscoelastic hydrogel, easy to manipulate, potentially biocompatible and biodegradable [19–21]. In the last decade, dextran and pullulan have demonstrated their suitability in tissue engineering of various organs and tissues, and have been successfully implanted in rodents and large animals without inducing any major inflammatory response [22–27]. These materials have recently been approved for a clinical trial in bone regeneration [28].

Our team has patented a fabrication technique of pullulan and dextran hydrogels based on the combination of porogen addition and freeze-drying process which leads to a high porosity and pore interconnectivity to allow optimal cell infiltration and maximize cell density. This is a low-cost good manufacturing practice (GMP) compatible method in water to easily produce, at a large-scale, porous scaffold with long-term storage at room temperature. Recently, we described the first proof of concept of its use for liver cells self-assembly to obtain reproducible hepatic 3D constructs with HepG2 cells [25]. Nevertheless, potential of pullulan-dextran hydrogel for hepatic cell differentiation, long-term viability, and *in vivo* liver functionality was not yet explored.

In the present work, using human bipotent HepaRG cell line, we provide a strategy for the efficient generation and differentiation of self-assembled functional 3D hepatic constructs within porous pullulan-dextran hydrogel. By *in vitro* and *in vivo* approaches, we demonstrate maintenance of long-term structure and functions of liver cell 3D structures, such as the presence of bile canaliculi and functional detoxification system. Finally, we demonstrate for the first time, liver biocompatibility and survival advantage in acetaminophen (APAP)-induced liver failure of pullulan-dextran hydrogel loaded with HepaRG 3D structures. These findings highlight pullulan-dextran hydrogel potential value for LTE with promising outcomes for the treatment of ALF upon implantation.

2. Materials and methods

2.1. Porous hydrogel synthesis

Pullulan (MW 200 000 Da) and dextran (MW 500 000 Da) were obtained from Hayashibara Inc, Okayama, Japan and Pharmacosmos respectively. Sodium trimetaphosphate (STMP) was provided by Sigma Aldrich, fluorescein isothiocyanate FITC-dextran (MW 500 000 Da, TdB Consultancy) was used to label the hydrogels.

Hydrogels were prepared as previously described [25]. Briefly, a mixture of pullulan and dextran with a ratio 75:25 was prepared in distilled water. For some analysis, 1% FITC labelled dextran 500 000 Da was added to the solution. Sodium chloride (NaCl) was incorporated into this solution prior to cross-linking under alkaline conditions (1 M sodium hydroxide (NaOH)) using 3% (w/v) STMP at 50 °C for 20 min. The resulting gel was cut into the desired shape (5 mm diameter, 1 mm thickness) before being immersed in 10X PBS and washed extensively with distilled water. Finally, hydrogels were freeze-dried as previously described in NaCl 0.025% for long-term storage and absorption properties during cell culture [29].

2.2. Cell culture and HepaRG cells 3D structures formation in hydrogel

Proliferating HepaRG™ hepatoma-derived cell line, HPR101 - Undifferentiated HepaRG™, were purchased from Biopredic International. Cells were amplified for two weeks prior to use under Biopredic International standard cell culture conditions as previously described [7]. For 3D structure self-assembly, cell loading into hydrogel was performed using syringe-induced vacuum. Briefly, all freeze-dried hydrogels were introduced in a syringe along with HepaRG cell suspension. Vacuum was induced by moving a plunger until fully impregnation of hydrogel. Basal media was maintained 7 days until obtention of self-aggregated HepaRG cells. Then, 2% (vol/vol) dimethyl sulfoxide (DMSO)-containing medium was added for 14 days (differentiation condition) in order to promote expression of differentiated hepatic markers and functions, as previously described [7]. In parallel, some hydrogels were maintained in basal DMSO free medium for 14 days (basal conditions).

2.3. Further applied methods

Further animal procedures immunohistochemistry, biochemical and cell activity protocols are described in details in the supplementary methods.

3. Results and discussion

3.1. Self -assembly and viability of HepaRG 3D structures in the hydrogel

As there are no existing guidelines for the induction of HepaRG cell differentiation in 3D porous hydrogel, the first challenge was to establish an optimal culture method to obtain functional microtissue in 3D conditions. HepaRG cells were expanded for 2 weeks in 2D culture and subsequently seeded into pullulan-dextran hydrogel (Hyd) by vacuum-induced impregnation, as previously described for HepG2 cells [25]. Then, basal medium was maintained for 7 days to reach the final size and immobilization of HepaRG cells 3D structures (Fig. 1 A). DMSO-containing medium was added for 14 days to induce cells differentiation [7], and *in vitro* results were compared with scaffolded HepaRG cells 3D structures cultivated in basal medium.

In order to support liver functions *in vivo*, we maximized the number of transplanted 3D cells structures [2,6,30]. Our results suggest that pullulan-dextran hydrogel could be a good candidate for transplantation of biomaterial-containing spheroids due to its high loading capacity, with approximatively 3800 HepaRG cells 3D structures formed per Hyd from 1 million seeded cells (Fig. 1 B). In fact, our pullulan-dextran hydrogel could contain 1 million cells in absolute value, i. e 20 million cells/ml. This is 10–20 times higher than most of the hydrogels in the literature that were loaded with 50 000 to 100 000 cells in absolute value [11,14,15,31,32]. Size of the 3D liver construct should be carefully designed, as spheroids/organoids diameter should not exceed 150 μm to prevent necrotic core formation [33–35]. Size analysis from phalloidin staining after 21 days revealed a majority of 3D structures presenting diameters under 100 μm (mean volume = 523.598,78 μm^3) (Fig. 1 B) and no HepaRG cells 3D structures presenting a diameter higher than 150 μm were found (mean volume = 1.767.145,87 μm^3), both in basal and differentiation culture conditions. Our data demonstrate efficient mass loading with consistent shape and size of 3D structures. This observation

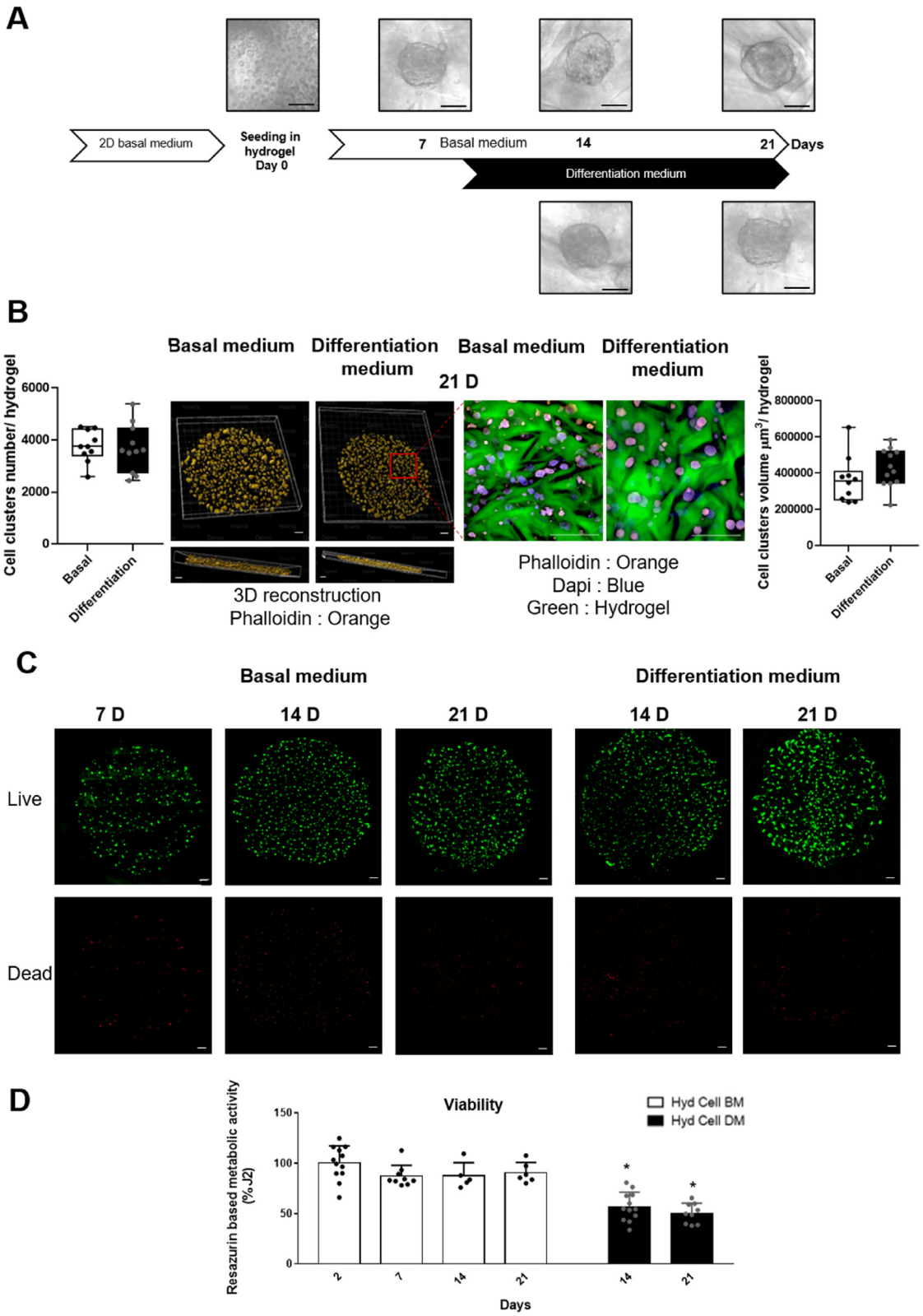

Fig. 1. HepaRG cells 3D structures formation and viability in hydrogel (A) HepaRG cells self-assembly production and differentiation protocol. Scale bar 50 µm. (B) HepaRG cells in hydrogel after 21 days of culture under basal and differentiation conditions. From left to right: cells cluster number, 3D reconstruction with IMARIS software of representative images of cell clusters in one hydrogel (phalloidin in orange); confocal representative images of hydrogels-FITC loaded with HepaRG cells (phalloidin in orange and nuclei in blue); volume of cluster. Number and volume were determined using a 3D semi-automatic analysis using Imaris software. n = 10 (basal) - 12 (differentiation) per group. Scale bar: 500 µm. Whiskers show min to max values. (C) Representative 3D images of live-dead analysis. Living cells were stained with Calcein AM (green) and dead cells are detected with Ethidium homodimer (red). Scale bar 500 µm. (D) Resazurin based metabolic activity of HepaRG 3D structures in hydrogel expressed as 2 days culture percentage. * Represent Mann Whitney test statistical difference ($p < 0.05$) between basal (n = 5–12) and differentiation media (n = 9–12).

fits well with our previous work that showed more than 30% of porosity, and formation of small and ovoid HepG2 spheroids [25].

Even if no significant difference between culture conditions was observed, the volume of cell clusters cultivated in differentiation media was higher than those cultivated in basal media, and volume distribution appeared more homogeneous although not significantly different (Fig. 1 B).

In line with these results, undifferentiated and differentiated HepaRG cells 3D structures exhibited long term viability, as demonstrated by live/dead and metabolic activity analysis over 21 days (Fig. 1C & D). Interestingly, 7 days after the induction of differentiation, the metabolic activity decreased by half compared to the basal condition (Fig. 1 D), while live/dead staining revealed similar number of dead cells (less than 3%) in both condition (Fig. 1C and Supplementary Fig. 1 A). This result indicated that the reduced metabolic activity was not related to cellular death. One possible explanation could be a reduction of mitochondrial metabolism by DMSO addition and changes in mitochondrial metabolism during differentiation of hepatocyte progenitors into mature hepatocytes [36–38] in our pullulan-dextran Hyd. Oxygen diffusion and stiffness of cellular microenvironment that may contribute to reduced viability, cellular stress and phenotypical aberration [15,31,32,34,39–42] were also similar (Supplementary Fig. 1 B and C). In the present work, the local stiffness measured using microindentation was similar to the values also described for liver in the literature using indentation (between 4 and 11 kPa for healthy liver) [43] [–] [46]. In conclusion, the liver scaffolds developed here mimic the mechanical properties of the healthy liver. Thus, our results indicate maintenance of Hyd structure and elasticity over time with or without cells (Supplementary Fig. 1C), an interesting feature for long-term cultivation required for tissue engineering studies, especially with hepatic stem cells [2]. Our results confirmed that pullulan-dextran Hyd could be an appropriate candidate for long-term stability and viability of self-assembly 3D liver microtissue with limited degradation *in vitro*.

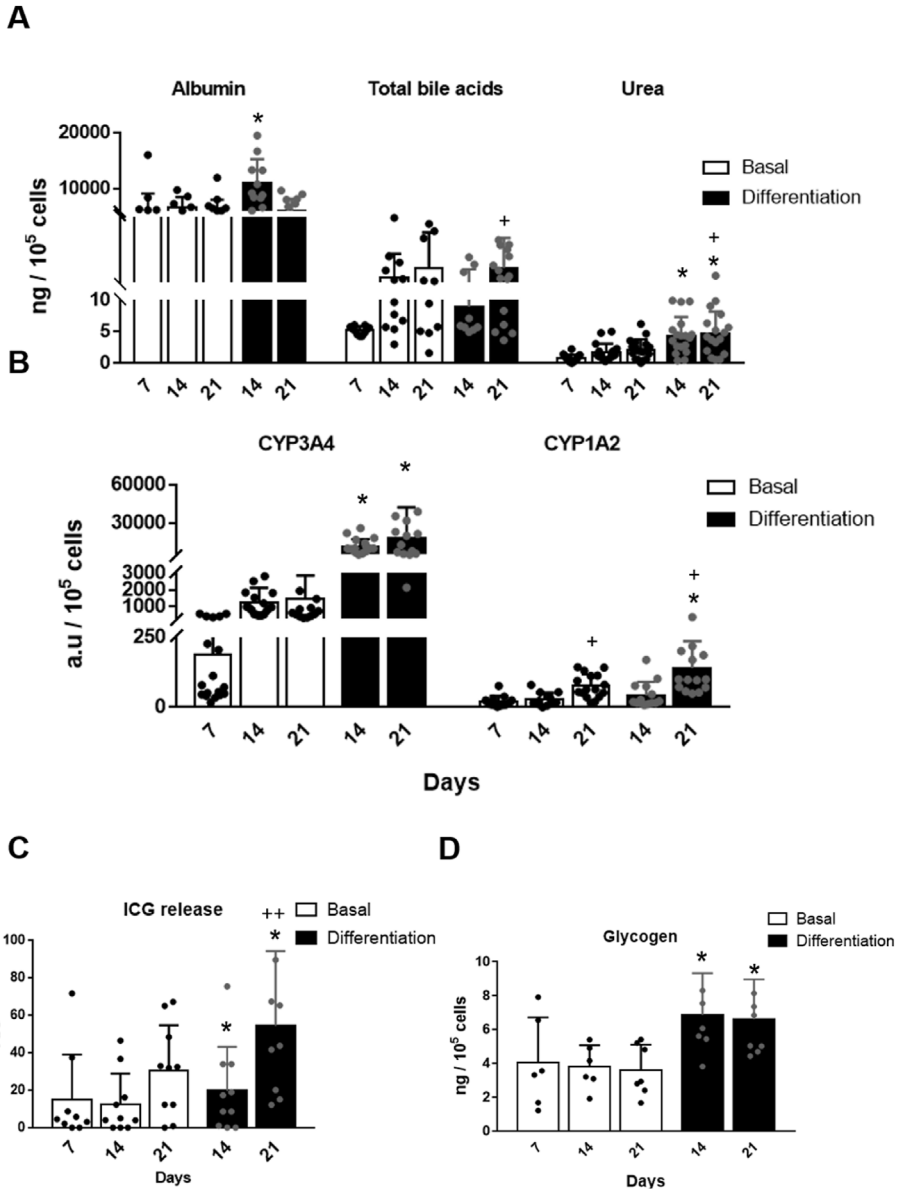

Fig. 2. HepaRG cells 3D structures hepatic activity in hydrogel (A) Albumin, total bile acids and urea release; (B) CYP3A4 and CYP1A2 activity (luciferin-based assay); (C) Indocyanine green release and glycogen content (D) after 2 h in hydrogel. * Represent statistical difference (*$p < 0.05$, **$p < 0,01$) between basal ($n = 6–18$) and differentiation ($n = 10–18$) medium at a same time, and + between time points of the same group with Mann-Whitney test analysis.

3.2. HepaRG cells 3D structures in the hydrogel demonstrate relevant hepatic functions

Typical hepatocyte mature functions of HepaRG cells 3D structures in Hyd are summarized in Fig. 2. Notably, human albumin secretion was detected at day 7 and remained noticeable during 21 days (Fig. 2 A). Cell supernatant revealed that HepaRG cells secreted bile acids and urea from 7 to 21 days (Fig. 2 A), indicating the ability of hepatocytes to excrete biological waste [47]. Under physiological conditions, the urea-cycle is the preferred route for ammonia fixation, as urea itself is not toxic and easily excreted by the kidney [47]. We found urea production by undifferentiated or differentiated HepaRG cells in pullulan-dextran Hyd. The functionality of bile canaliculi was investigated using 5 (6)-Carboxy-2′, 7′-dichlorofluorescein diacetate (CDFA) experiment. In hepatocytes, CDFA enters passively and is hydrolyzed by intracellular esterases, then CDF is metabolized and actively excreted into the bile canaliculi by MRP2 transporter. This active transport was monitored using live fluorescence microscopy that showed a progressive clearance of CDF from the cytosol concomitant to its accumulation between cells (Supplementary Fig. 2 A). This result is in agreement with the localization of transporters staining showed in Supplementary Fig. 3. These data suggest that MRP2 and the excretion system are functional in our Hyd.

The drug detoxification capability was also assessed by measuring the activities of the major cytochrome P450 enzymes responsible for the oxidative metabolism of drugs in the human liver, namely CYP3A4 and CYP1A2 [48,49]. Cytochrome activities was confirmed, and an increase was observed when the cells were cultivated in differentiation medium (Fig. 2 B). Another main property of hepatocyte function is the capability to respond to compounds able to induce the biosynthesis of a toxic metabolite. The metabolic activity of the HepaRG cells was significantly increased when treated with low concentrations of hepatic toxic compounds, such as APAP and diclofenac (Supplementary Fig. 2 B). When increasing compound concentration, the metabolic activity decreased in a dose-dependent manner, suggesting cell death.

APAP is metabolized mainly by CYP2E1, CYP1A2, and CYP3A4 [48,49], but also by several other enzymes that could counteract its product toxicity, whereas diclofenac is metabolized mainly by CYP2C9 and CYP3A4, and their sensitivity is reduced when cells express low drug metabolizing enzyme activities [50,51]. Under differentiation condition, HepaRG cells response to APAP and diclofenac was more consistent, suggesting better CYPs pattern expression.

In the literature, 3D-cultured HepaRG cells demonstrated 0.5–3 μg albumin secretion and 1–5 ng urea for 10^5 cells, 5000–30 000 RLU/10^5 cells for CYP3A4 activity [11,14,40,52]. In our system we obtained 5–10 μg albumin, 5 ng urea and about 20 000 RLU CYP3A4 activity for 10^5 cells, suggesting 3D-cultured HepaRG cells in pullulan-dextran hydrogel are similarly functional. We also examined the cellular excretion of indocyanine green (ICG), an organic dye that is taken up, and subsequently eliminated specifically by hepatocytes. ICG was found in both media and upregulated upon addition of DMSO (Fig. 2C). The cellular uptake was observed in both conditions (Supplementary Fig. 2C), and almost completely disappeared 24 h later, indicating that the biotransformation system of HepaRG cells is highly functional when cultivated in pullulan-dextran Hyd.

Finally, glycogen content of HepaRG cells 3D structures was detected at day 7 and remained notable during 21 days (Fig. 2 D, Supplementary Fig. 2 D). In line with previous results, differentiated HepaRG store more glycogen compared to undifferentiated ones, suggesting a more effective carbohydrate metabolism.

Our data demonstrate typical hepatocyte mature functions of self-assembled HepaRG cells 3D structures in Hyd, notably, albumin secretion, drug-metabolizing enzymes activity, bile acid production, excretion functional system and glycogen metabolism. Most of the functions previously described increased over time in DMSO-supplemented medium, suggesting the differentiation process acts properly on HepaRG cells 3D structures in pullulan-dextran Hyd.

Interestingly, we also provide data suggesting partial hepatocyte maturation without DMSO. Only few studies have shown the ability to differentiate HepaRG in 3D systems without DMSO, and this could represent an advantage for increasing the reliability and repeatability of toxicological *in vitro* experiments [9,52,53]. Taken together, these data confirm that our hydrogel promotes HepaRG self-assembly and differentiation into 3D hepatocytes structures which demonstrate suitable functionalities.

3.3. HepaRG cells 3D structures in the hydrogel differentiate and maintain cell polarity

HepaRG is a bipotent progenitor cell line able to produce two hepatic populations: hepatocyte-like and primitive biliary cells with the same culture medium, representing an interesting model for co-culture experiments [7,31,54]. Here, immunostaining of hepatocyte (HNF4α nuclear factor and albumin) and cholangiocyte (sox9) markers demonstrated the presence of hepatocyte cells and biliary-like cells in 3D structures after 21 days in differentiation medium (Fig. 3). Furthermore, some bipotent progenitors (CK19 and HNF4α) remained in the mature 3D hepatic structure (Fig. 3), as it occurs in native liver tissue [55]. *In vivo*, they could represent an advantage by acting as a pool of undifferentiated cells that undergo hepatocyte or biliary differentiation depending on the injury [55,56].

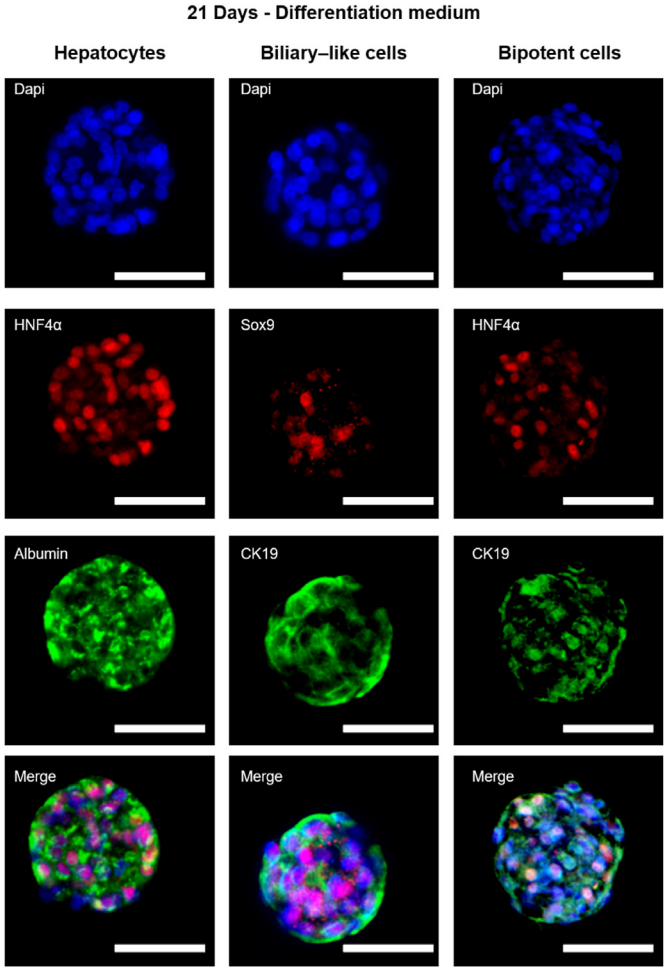

Fig. 3. HepaRG cells differentiation in hydrogel at day 21 in differentiation medium.
Hepatocytes (HNF4α, Albumin), biliary cells (CK19, SOX9) and bipotent cells (CK19 & HNF4α) markers expression. Scale bar 50 μm. Data representative of triplicate experiments.

Moreover, phalloidin staining revealed actin aggregates bounded to HepaRG cells coinciding with bile canaliculi structure of mature and functional hepatocyte (Supplementary Fig. 3) [57].

HepaRG differentiation is regulated at least in part by activation of mechano-transduction signals and is consequently affected by the stiffness of the environment [15,31,58]. For example, previous works have reported few or absence of biliary cell 3D differentiation when seeded in stiff hydrogels [11,31,32]. We speculate our hydrogel offers appropriate mechanical environment promoting HepaRG differentiation into both hepatocytes and biliary-like cells.

Mature hepatocytes are polarized with distinct apical/luminal domains (bile canaliculi) that are separated by tight junctions from the basolateral domain, formed by multiple basal surfaces facing the endothelial lining and sinusoidal blood. This polarity is crucial for hepatocyte functions [59]. MRP2, an apical (bile canaliculus) ATP-dependent multispecific organic anion transporter considered as a differentiation and polarity marker [60], colocalized with actin aggregates in our 3D cell structures (Supplementary Fig. 3). The tight junction-associated protein ZO1, the ATP-dependent bile salt transport export pump (BSEP), ABCB1 and MRP1 transporters were also concentrated at actin aggregates bounded (bile canaliculi) (Fig. 3 Supplementary Fig. 3, in agreement with normal hepatocyte polarity [59]. In addition, immunofluorescence staining revealed that the basolateral hepatic transporter OATP, which uptakes organic solutes from sinusoidal blood, did not colocalize with bile canaliculi delimited by actin concentrated aggregates. The same localization was observed for Na^{+}-taurocholate cotransporting polypeptide NTCP, the main basolateral bile salt transporter [59]. These results confirm the correct expression and localization of polarity markers of HepaRG cells 3D structures in Hyd, and thus differentiation into mature hepatocytes.

Immunostaining experiments also indicated some connections between HepaRG cells 3D structures present in different pores of the hydrogel (Supplementary Fig. 4 A). These bridges between 3D cells structures were functional and allowed communication between them as indicated by CDFA experiments (Supplementary Fig. 4 B). Even if precise mechanisms involved in 3D cell structures communication need to be further explored, networked ones could provide a higher degree of function and organization [61]. Taken together, these data argue for the formation of abundant HepaRG cells self-assembly into 3D structures that exhibit *in vivo*-like cellular arrangement and functionality for at least 14 days in media supplemented with DMSO, and therefore highlight the interest of using pullulan-dextran Hyd for 3D liver model.

3.4. HepaRG cells 3D structures in hydrogel are liver biocompatible and remain implanted for one month

Pullulan-dextran cellularized Hyds have demonstrated good biocompatibility and suitable degradation times after engraftment in dorsal subcutaneous murine models [22–27]. However, their biocompatibility when seeded with hepatocytes in soft tissues with highly active metabolism was unknown. To this purpose, HepaRG cells in Hyd were implanted easily on top of the left and right liver lobes in immunocompromised mice then, a drop of fibrinogen-based surgical glue was applied around the biomaterial before relocating median lobes on top.

Surgical procedure and HepaRG implantation did not induce increased mice mortality nor liver injury or fibrotic scar after 28 days (Fig. 4A–C). Moreover, HepaRG cells in Hyd maintained their position over 1 month after implantation and signs of hydrogel biodegradation were obvious with a reduction of the graft size and host liver integration of Hyd (impossibility to separate them from each other; data not shown), suggesting degradation in healthy hepatic tissue.

In the light of previous studies suggesting that biomaterials integration into the liver could be assigned to increased inflammatory or fibrogenic response in the recipient organ [62,63], we analyzed typical liver matrix remodeling and inflammatory factors. Mice transplanted with HepaRG cells in Hyd and sham exhibited similar mRNA expression levels for profibrogenic (Col1α1, αSMA), matrix remodeling (MMP13, MMP2, MMP9, TIMP-1), and proinflammatory (TNFα, IL-6, IL-1β, NOS2, MCP1, F4/80, LY6G) markers one month after transplantation (Fig. 4C and Supplementary Fig. 5). Neither aberrant hepatocyte proliferation (and Supplementary Fig. 5 A, Ki67), nor ductular reaction (Supplementary Fig. 5 B, CK19) in the recipient liver were found. These data suggested that interaction between hydrogel and surrounded recipient liver did not induce unwanted liver injury nor transplant rejection. We speculate that the mechanical properties of our hydrogel being within the range of healthy human liver tissue [43–46,64] (Young modulus between 3 and 10 kPa as measured by Nanoindentation, Supplementary Fig. 1) allow this host integration. Even if further studies are needed to explore the kinetics of pullulan-dextran degradation in liver with or without injury, our findings argue for appropriate liver biocompatibility of pullulan-dextran Hyd loaded with HepaRG 3D cells structures.

One major challenge for engineered liver is the limited viability after engraftment and ability to mimic its *in vivo* counterparts. Human albumin in the sera of transplanted and non-transplanted mice was measured every week during one-month post-engraftment (Fig. 4 D). Human albumin was detected at high levels in every implanted mouse after 7 days, confirming the survival and engraftment of HepaRG cells in the hydrogel. After 14 days, albumin expression decreased by 10-fold, suggesting cell death. This decrease is in agreement with the 10% cell engraftment without biomaterial scaffold after implantation in rodents reported by others [6,30,65]. It must be noted that for an efficient engraftment of hepatic cells, a sustained liver damage with an important rate of cell death seems necessary [66–68]. Nonetheless, human albumin remained stable during the 3 following weeks suggesting that the grafted cells did not suffer from oxygen and nutriment deprivation and were well incorporated in mice.

Interaction between hydrogel and liver, as well as HepaRG 3D cells structures in hydrogel, were identified using immunodetection (Fig. 4 E). Invagination of liver in hydrogel observed by confocal microscopy (Fig. 4 E upper panel) confirmed the integration of cell-seeded hydrogel into the host liver. Moreover, cells in the hydrogel remained in ovoid structures 28 days after implantation, with only few individual living or dead cells (Fig. 4 E). In agreement with this observation, HepaRG cells 3D structures expressing albumin and presenting canaliculi-like structures were observed (Fig. 4 E lower panel). These results support that human albumin found in mice sera was produced by the 3D cells structures and not by individual cells.

In the literature, it is suggested that coculture with endothelial or stromal cells may be necessary to enhance hepatocyte functionality and/or to prolong cell survival mediated by vascularization after implantation [31,69–71]. However, optimal cell source and cellular composition remains poorly delineated and some coculture studies of endothelial cells and hepatocytes demonstrated long-term integration but no functional advantage *in vivo* [72,73]. Interestingly, our results demonstrate successful long-term implantation, survival and function of HepaRG cells 3D structures *in vivo*. This observation highlights the complex influence of cell signals in physiologically environment and the need of further studies exploring pullulan-dextran Hyd and host interaction.

Nevertheless, implantation procedure results support biocompatibility, integration and functionality of pullulan-dextran Hyd as a microtissue self-assembly platform.

3.5. HepaRG cells 3D structures in hydrogel offer therapeutic potential after acute liver injury

Aiming to assess the therapeutic potential of HepaRG cells 3D structures *in vivo*, we used the relevant model of APAP toxicity in immunocompromised mice, which mimics ALF. This model induces consistent hepatotoxicity, and hepatocyte damage occurs at doses that are similar to those reported to induce damage in human liver [74], while being compatible with the surgical procedure required for implantation. In this procedure, two additional hydrogels with HepaRG cells were implanted

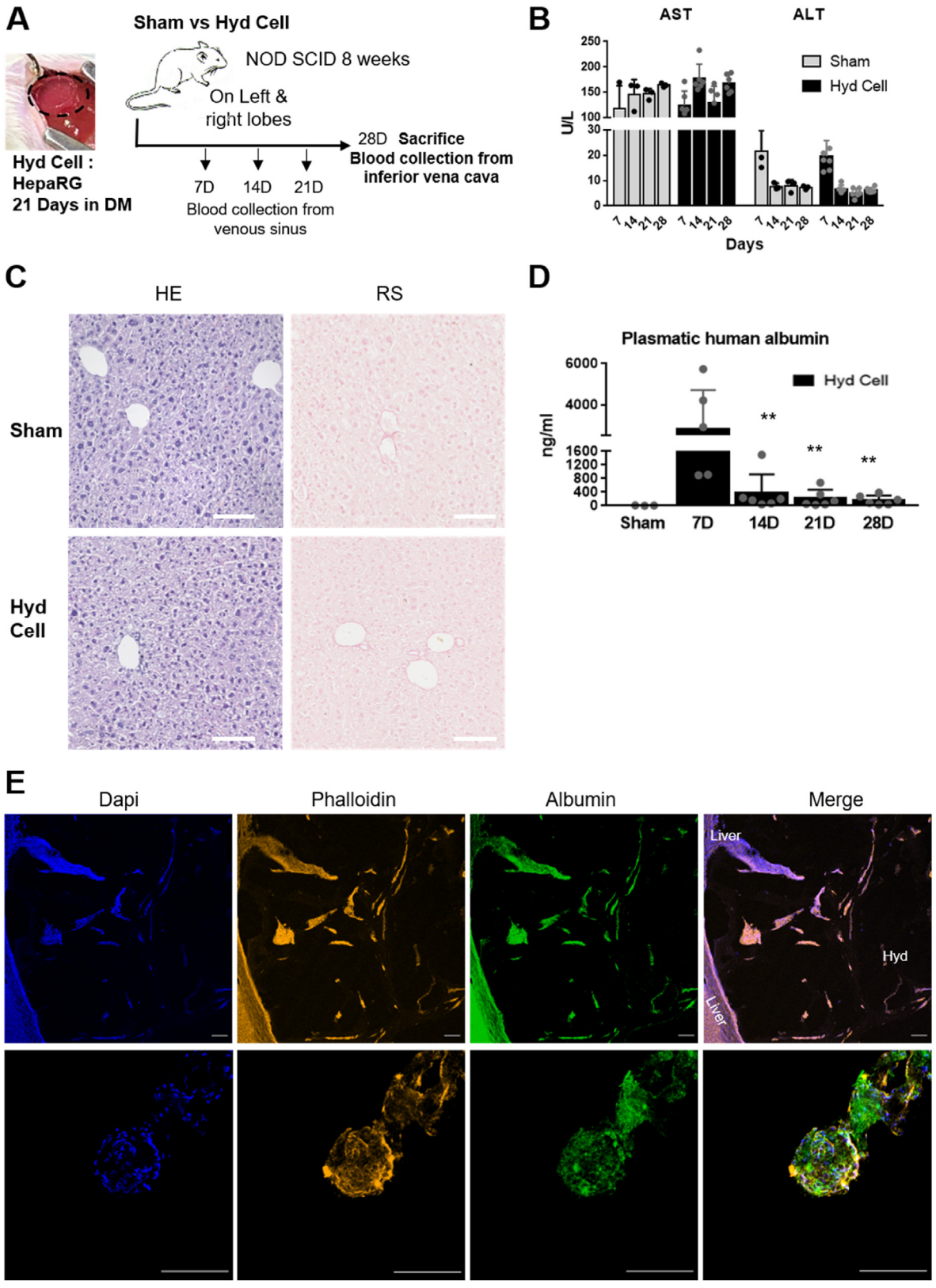

Fig. 4. In vivo liver biocompatibility of HepaRG cells 3D structures in hydrogel (A) Implantation procedure. (B) Plasmatic transaminases dosages over time. (C) Representative images of hematoxylin and eosin (HE) and sirius red (SR) of host liver 28 days after implantation. White circles highlight Ki-67 positive cells (D) Plasmatic human albumin concentration in mice. (E) Top: Phalloidin (orange) and albumin (green) staining of hydrogel implant grafted on the liver. Bottom: Phalloidin (orange) and albumin (green) staining of HepaRG cells in the implant after 28 days. Scale bar 100 μm. Sham n = 3, Hyd Cell n = 6.

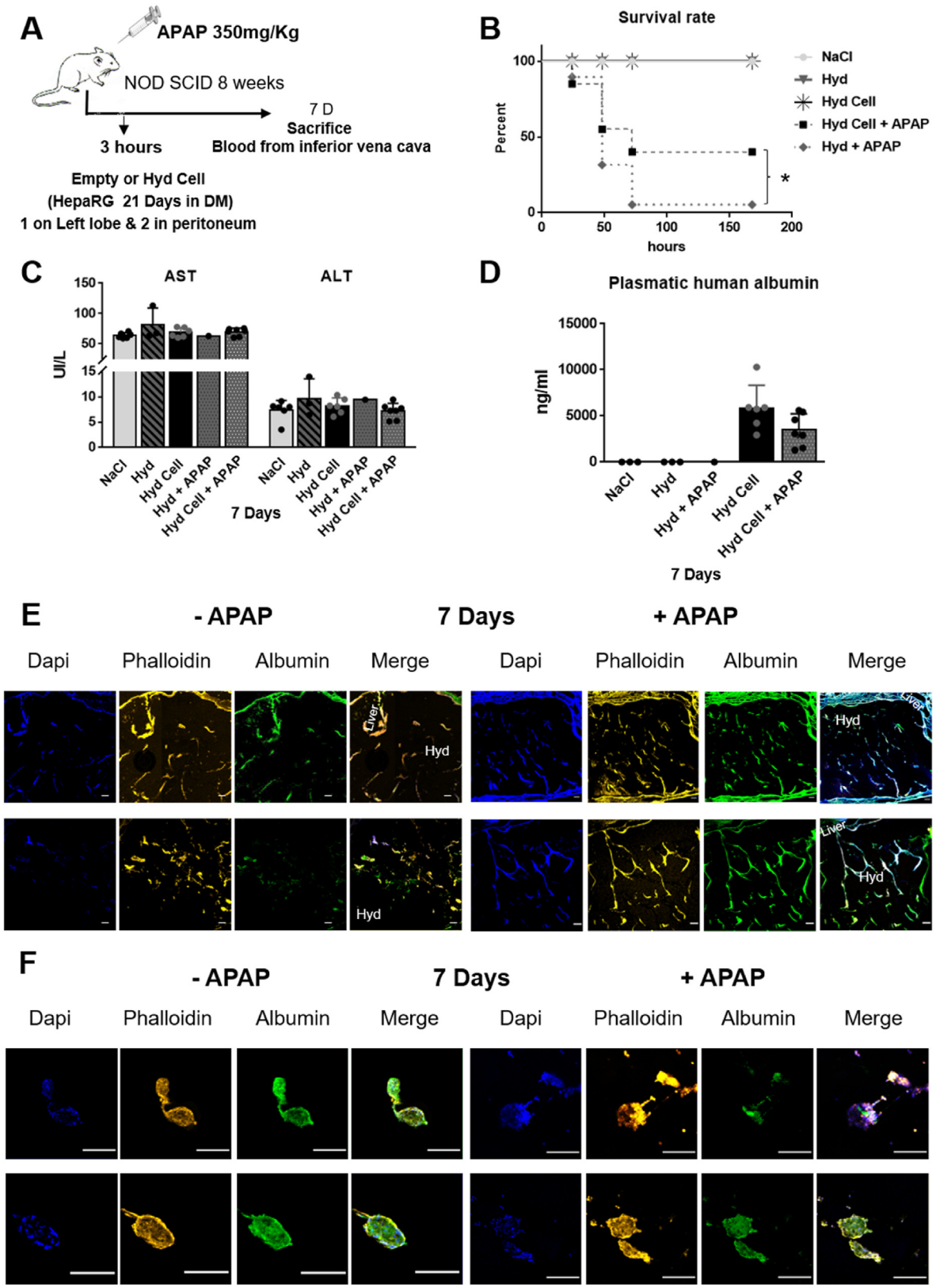

Fig. 5. HepaRG cells 3D structures in hydrogel therapeutic effect after APAP induced acute liver injury (A) Schematic representation of APAP induced acute liver injury in mice and hydrogel implantation. (B) Mice survival rate after 350 mg/kg APAP toxic challenge. n = 19 Hyd Cell + APAP, n = 20 Hyd + APAP, n = 6 for NaCl and Hyd Cell and N = 3 for Hyd. * Represent statistical difference ($p < 0,05$) with log-rank (mantel-cox) test analysis. (C) Plasmatic transaminases 7 days after APAP treatment and implantation. (D) Plasmatic human albumin concentration 7 days after APAP treatment and implantation. n = 1 for Hyd + APAP, n = 7 for Hyd + APAP, n = 6 for NaCl and Hyd Cell and n = 3 for Hyd * Represent statistical difference ($p < 0,05$) with Mann-Whitney test analysis. (E) Phalloidin (orange) and albumin (green) staining of hydrogel implant connecting the liver after 7 days with (right) or without (left) APAP treatment. (F) Phalloidin (yellow) and albumin staining of HepaRG 3D structures (F) damaged (upper) or not (down) by APAP in remaining implant at 7 days. Scale bar 100 μm.

in the peritoneal cavity to reach 3 million cells implanted per mice.

To induce a lethal overdose of APAP, a 12 h fasting period was applied to deplete hepatocytic glutathione levels, normally required to inactivate the toxic metabolite of APAP (Fig. 5 A). To this respect, without fasting period before APAP administration, mortality was very low, with only 10% of dead implanted mice with empty hyd (data not shown). Noteworthy, without APAP administration, implantation of hydrogels with (Hyd Cell) or without (Hyd) HepaRG cells or control injection (NaCl) did not induce mice death (Fig. 5 B).

In our *in vivo* experiments, 95% of implanted mice with non-cellularized Hyd died after APAP injection (Fig. 5B, Hyd + APAP). It is worth noting than 350 mg/kg intraperitoneal injection of APAP in the literature induces the death of 0–70% of rodents depending on fasting period, sex, age, genetic background and phenotypes [74–76]. Fasting period plus APAP induce hypoglycaemia and hypothermia [74,77]. Implantation of scaffolds also required an additional surgical procedure. Thus, we obtained in these conditions a lethal synergistic effect of APAP administration and the subsequent surgical procedure. Using this model, we could challenge the therapeutic potential of HepaRG 3D cells in pullulan-dextran hydrogel to support liver function during an ALF. Indeed, only 5% of the Hyd-transplanted animals without HepaRG cells survived 3 days after APAP administration (Hyd + APAP), whereas survival rate was 36.8% for the animals transplanted with Hyd-HepaRG 3D cells (Hyd Cell + APAP), indicating a clear survival advantage (Fig. 5 B) for mice receiving cell therapy. This result demonstrates that implanted HepaRG cell 3D structures in Hyd support liver functions *in vivo* during an injury, and thus prevent mice death by liver failure. Besides, survivor mice fully recovered from APAP-induced liver injury by 7 days after injection (Fig. 5C), suggesting that the surgical implantation after APAP treatment did not delay normal liver regeneration.

When mice hepatocytes were seeded in PLGA scaffold, results similar to ours were reported with 31.6% of animals survival in galactosamine-induced lethal liver injury but with at least 10 million cells [69]. In another study, intraperitoneal transplantation of alginate micro-encapsulated rat hepatocytes reduced the severity of liver damage, but did not improve the survival rate in galactosamine-induced liver injury [78]. In the same line, bioprinted LO2 cell spheroids improved the liver function and only prolonged the survival times by one month after radiation-induced liver damage combined with a partial hepatectomy [79]. Finally, HepaRG bioprinted with gelatin and alginate alleviated injury of the liver in a murine model of tyrosinemia [80]. In those studies, hepatocyte implantation prolonged the survival of animals but did not confer a survival advantage [79,80]. In the same model, embryonic hepatic cell lines scaffolded in polycaprolactone blunt liver damage, however, the preventive implantation approach that was chosen cannot be transferred to the clinic [81]. Finally, contrasting with our results, another study suggested no beneficial effect on liver cirrhosis in rats transplanted with collagen fiber-based scaffold with 3D mice hepatocyte spheroids [82]. All these studies support the importance of selecting the adequate cell source and number in a relevant pathological model. They also highlight the difficulty to compare biomaterials and cells activity between studies due to large differences in the study design.

Transplanting an efficient liver mass is essential for clinical application. To ensure liver functions during liver failure by individual hepatocytes, administering the equivalent of 5–12% of the whole liver mass is required [2,6,30]. In our model, although we used about 3 million cells per mice, corresponding to only 1.5–2% of the mouse hepatocyte mass, this was sufficient to rescue 36.8% of the animals. This suggests that HepaRG cells in pullulan-dextran Hyd are efficient *in vivo* to support liver function during toxic injury. Human albumin in mice sera was detected here 7 days after APAP treatment (Fig. 5 D). Immunostaining on sections of hydrogel linked to liver lobe after APAP treatment revealed HepaRG cell 3D structure reorganization and an enhanced invagination of the host liver cells into hydrogel than with no liver injury, suggesting a better communication between them (Fig. 5 E upper panel). Upon APAP administration, more infiltrated cells and less ovoid HepaRG cells 3D structures were noticed (Fig. 5 E lower panel). 3D clusters presented loss of structure, necrosis area and/or loss of albumin expression (Fig. 5 F upper panel) compared to those not treated with APAP (Fig. 5 F lower panel). The same observations were made in hydrogels implanted in the peritoneal cavity (data not shown). As they became blurry with very high background due to the body fluids absorbed during the laparotomy, we did not provide staining. These results fit well with the reduced human albumin content in sera after APAP administration and HepaRG cell death (Fig. 5D, p-value =0,0513). One possible explanation could be paracrine death signal from the suffering host liver to the implant. However, increased mice survival rate with engineered liver transplantation and presence of some HepaRG cells 3D structures albumin positive presenting bile canaliculi-like structure (Fig. 5 E lower panel) argue for a maintenance of HepaRG cells hepatic functions in pullulan-dextran Hyd after APAP-induced injury. Long-term survival of cells and their fate in the implant after APAP-induced injury need to be further investigated with clinically approved cells to confirm therapeutic potential use of cellularized pullulan-dextran hydrogel in ALF.

New perspectives to improve self-assembly 3D liver microtissue and broaden their applications can be pointed out. Material shape and/or thickness could be modified for optimized graft implantation to allow a better connection with the liver and/or blood circulation, or to obtain a higher degree of liver structure that could enhance their clinical impact [61,73]. To avoid a major surgical procedure, integrating our cellularized hydrogel into an extracorporeal liver bioartificial system could be considered [2,4,5].

4. Conclusion

In summary, we can easily prepare GMP biocompatible porous pullulan-dextran hydrogels with a time and cost-effective procedure and successfully engineer stable and functional 3D liver-like tissue *in vitro*. Hydrogel loaded with HepaRG cells 3D structures transplanted *in vivo* revealed good liver biocompatibility and survival advantage upon toxic injury. Together with *in vitro* experiments, these data provide a first and robust preclinical proof of concept towards the use of cellularized pullulan-dextran hydrogel as an alternative platform to donor transplant for human liver failure management and treatment.

Author contributions

Funding and study supervision: DL, TSY; Study design: CLG, TSY, DL; Animal studies design: CLG, GM, TT; Data acquisition: CLG, GM, AD, MNL, RA, TT; Data analysis: CLG; Writing—original draft preparation: CLG; writing—review and editing: CLG, GM, AD, MNL, RA, TT, DL, TSY. All authors have read and agreed to the published version of the manuscript.

Funding

This research was funded by “Recherche Hospitalo-Universitaire” Innovations for Liver Tissue Engineering (RHU iLite), grant number ANR-16-RHUS-0005. Works from the Laboratory U1148 are supported by Inserm, Université Sorbonne Paris Nord, and Université Paris Cité.

Declaration of competing interest

The authors declare the following financial interests/personal relationships which may be considered as potential competing interests:Didier Letourneur reports financial support was provided by French National Research Agency. Didier Letouneur reports a relationship with SILTISS that includes: equity or stocks. Didier Letourneur has patent issued to Assignee. DL has shares in SILTISS company that acquired from INSERM four patents related to the production of polysaccharide scaffolds for tissue engineering.

Data availability

Data will be made available on request.

Acknowledgements

We thank Samira Benadda of the CRI U1149 Imaging facility, the Central Animal Facility of Université Paris Cité, Dr Soraya Lanouar and Jean-Philippe Tosiani for technical support and fruitful discussions. We thank Servier Medical Art image bank and BioRender that were used to create graphical abstract.

Appendix A. Supplementary data

Supplementary data to this article can be found online at https://doi.org/10.1016/j.mtbio.2023.100554.

References

[1] R. Moreau, B. Gao, M. Papp, R. Bañares, P.S. Kamath, Acute-on-chronic liver failure: a distinct clinical syndrome, J. Hepatol. 75 (Suppl 1) (2021), https://doi.org/10.1016/j.jhep.2020.11.047. S27–S35.
[2] G. Mazza, W. Al-Akkad, K. Rombouts, M. Pinzani, Liver tissue engineering: from implantable tissue to whole organ engineering, Hepatol. Commun. 2 (2018) 131–141, https://doi.org/10.1002/hep4.1136.
[3] N. Prior, P. Inacio, M. Huch, Liver organoids: from basic research to therapeutic applications, Gut 68 (2019) 2228–2237, https://doi.org/10.1136/gutjnl-2019-319256.
[4] G.H. Underhill, S.R. Khetani, Bioengineered liver models for drug testing and cell differentiation studies, Cell. Mol. Gastroenterol. Hepatol. 5 (2017) 426–439.e1, https://doi.org/10.1016/j.jcmgh.2017.11.012.
[5] J. Zhang, X. Zhao, L. Liang, J. Li, U. Demirci, S. Wang, A decade of progress in liver regenerative medicine, Biomaterials 157 (2018) 161–176, https://doi.org/10.1016/j.biomaterials.2017.11.027.
[6] A. Dhawan, J. Puppi, R.D. Hughes, R.R. Mitry, Human hepatocyte transplantation: current experience and future challenges, Nat. Rev. Gastroenterol. Hepatol. 7 (2010) 288–298, https://doi.org/10.1038/nrgastro.2010.44.
[7] P. Gripon, S. Rumin, S. Urban, J. Le Seyec, D. Glaise, I. Cannie, C. Guyomard, J. Lucas, C. Trepo, C. Guguen-Guillouzo, Infection of a human hepatoma cell line by hepatitis B virus, Proc. Natl. Acad. Sci. U.S.A. 99 (2002) 15655–15660, https://doi.org/10.1073/pnas.232137699.
[8] V. Cerec, D. Glaise, D. Garnier, S. Morosan, B. Turlin, B. Drenou, P. Gripon, D. Kremsdorf, C. Guguen-Guillouzo, A. Corlu, Transdifferentiation of hepatocyte-like cells from the human hepatoma HepaRG cell line through bipotent progenitor, Hepatol. Baltim. Md 45 (2007) 957–967, https://doi.org/10.1002/hep.21536.
[9] M. Mandon, S. Huet, E. Dubreil, V. Fessard, L. Le Hégarat, Three-dimensional HepaRG spheroids as a liver model to study human genotoxicity in vitro with the single cell gel electrophoresis assay, Sci. Rep. 9 (2019), 10548, https://doi.org/10.1038/s41598-019-47114-7.
[10] S.C. Ramaiahgari, S.S. Ferguson, Organotypic 3D HepaRG liver model for assessment of drug-induced cholestasis, Methods Mol. Biol. Clifton NJ (1981) 313–323, https://doi.org/10.1007/978-1-4939-9420-5_20, 2019.
[11] Y. Higuchi, K. Kawai, T. Kanaki, H. Yamazaki, C. Chesné, C. Guguen-Guillouzo, H. Suemizu, Functional polymer-dependent 3D culture accelerates the differentiation of HepaRG cells into mature hepatocytes, Hepatol. Res. Off. J. Jpn. Soc. Hepatol. 46 (2016) 1045–1057, https://doi.org/10.1111/hepr.12644.
[12] P. Gunness, D. Mueller, V. Shevchenko, E. Heinzle, M. Ingelman-Sundberg, F. Noor, 3D organotypic cultures of human HepaRG cells: a tool for in vitro toxicity studies, Toxicol. Sci. Off. J. Soc. Toxicol. 133 (2013) 67–78, https://doi.org/10.1093/toxsci/kft021.
[13] M.N. Ashraf, M.W. Asghar, Y. Rong, M.R. Doschak, T.K.L. Kiang, Advanced in vitro HepaRG culture systems for xenobiotic metabolism and toxicity characterization, Eur. J. Drug Metab. Pharmacokinet. 44 (2019) 437–458, https://doi.org/10.1007/s13318-018-0533-3.
[14] M. Sun, J.Y. Wong, B. Nugraha, A. Ananthanarayanan, Z. Liu, F. Lee, K. Gupta, E.L.S. Fong, X. Huang, H. Yu, Cleavable cellulosic sponge for functional hepatic cell culture and retrieval, Biomaterials 201 (2019) 16–32, https://doi.org/10.1016/j.biomaterials.2019.01.046.
[15] M.M. Malinen, L.K. Kanninen, A. Corlu, H.M. Isoniemi, Y.-R. Lou, M.L. Yliperttula, A.O. Urtti, Differentiation of liver progenitor cell line to functional organotypic cultures in 3D nanofibrillar cellulose and hyaluronan-gelatin hydrogels, Biomaterials 35 (2014) 5110–5121, https://doi.org/10.1016/j.biomaterials.2014.03.020.
[16] S. Ye, J.W.B. Boeter, L.C. Penning, B. Spee, K. Schneeberger, Hydrogels for liver tissue engineering, Bioeng. Basel Switz. 6 (2019) E59, https://doi.org/10.3390/bioengineering6030059.
[17] A. da Silva Morais, S. Vieira, X. Zhao, Z. Mao, C. Gao, J.M. Oliveira, R.L. Reis, Advanced biomaterials and processing methods for liver regeneration: state-of-the-art and future trends, Adv. Healthc. Mater. 9 (2020), 1901435, https://doi.org/10.1002/adhm.201901435.
[18] E. Jain, A. Damania, A. Kumar, Biomaterials for liver tissue engineering, Hepatol. Int. 8 (2014) 185–197, https://doi.org/10.1007/s12072-013-9503-7.
[19] A. Autissier, C. Le Visage, C. Pouzet, F. Chaubet, D. Letourneur, Fabrication of porous polysaccharide-based scaffolds using a combined freeze-drying/cross-linking process, Acta Biomater. 6 (2010) 3640–3648, https://doi.org/10.1016/j.actbio.2010.03.004.
[20] D.B. Maurel, M. Fénelon, R. Aid-Launais, L. Bidault, A. Le Nir, M. Renard, J.-C. Fricain, D. Letourneur, J. Amédée, S. Catros, Bone regeneration in both small and large preclinical bone defect models using an injectable polymer-based substitute containing hydroxyapatite and reconstituted with saline or autologous blood, J. Biomed. Mater. Res. A. 109 (2021) 1840–1848, https://doi.org/10.1002/jbm.a.37176.
[21] S. Lanouar, R. Aid-Launais, A. Oliveira, L. Bidault, B. Closs, M.-N. Labour, D. Letourneur, Effect of cross-linking on the physicochemical and in vitro properties of pullulan/dextran microbeads, J. Mater. Sci. Mater. Med. 29 (2018) 77, https://doi.org/10.1007/s10856-018-6085-x.
[22] M. Lavergne, M. Derkaoui, C. Delmau, D. Letourneur, G. Uzan, C. Le Visage, Porous polysaccharide-based scaffolds for human endothelial progenitor cells, Macromol. Biosci. 12 (2012) 901–910, https://doi.org/10.1002/mabi.201100431.
[23] G. Gerschenfeld, R. Aid, T. Simon-Yarza, S. Lanouar, P. Charnay, D. Letourneur, P. Topilko, Tuning physicochemical properties of a macroporous polysaccharide-based scaffold for 3D neuronal culture, Int. J. Mol. Sci. 22 (2021), 12726, https://doi.org/10.3390/ijms222312726.
[24] T. Simon-Yarza, M.-N. Labour, R. Aid, D. Letourneur, Channeled polysaccharide-based hydrogel reveals influence of curvature to guide endothelial cell arrangement in vessel-like structures, Mater. Sci. Eng. C Mater. Biol. Appl. 118 (2021), 111369, https://doi.org/10.1016/j.msec.2020.111369.
[25] M.-N. Labour, C. Le Guilcher, R. Aid-Launais, N. El Samad, S. Lanouar, T. Simon-Yarza, D. Letourneur, Development of 3D hepatic constructs within polysaccharide-based scaffolds with tunable properties, Int. J. Mol. Sci. 21 (2020) E3644, https://doi.org/10.3390/ijms21103644.
[26] A. Abed, N. Assoul, M. Ba, S.M. Derkaoui, P. Portes, L. Louedec, P. Flaud, I. Bataille, D. Letourneur, A. Meddahi-Pellé, Influence of polysaccharide composition on the biocompatibility of pullulan/dextran-based hydrogels, J. Biomed. Mater. Res. A. 96 (2011) 535–542, https://doi.org/10.1002/jbm.a.33007.
[27] M. Chaouat, C. Le Visage, A. Autissier, F. Chaubet, D. Letourneur, The evaluation of a small-diameter polysaccharide-based arterial graft in rats, Biomaterials 27 (2006) 5546–5553, https://doi.org/10.1016/j.biomaterials.2006.06.032.
[28] Multicentre SILTISS, Interventional, Longitudinal, Open-Label Study Conducted in France Evaluating the Clinical Performance and Safety of Glycobone® as a Bone Filler in a Lateral Sinus Lift Setting, clinicaltrials.gov, 2022 (accessed June 15, 2022), https://clinicaltrials.gov/ct2/show/NCT05377710.
[29] J. Grenier, H. Duval, F. Barou, P. Lv, B. David, D. Letourneur, Mechanisms of pore formation in hydrogel scaffolds textured by freeze-drying, Acta Biomater. 94 (2019) 195–203, https://doi.org/10.1016/j.actbio.2019.05.070.
[30] B.J. Dwyer, M.T. Macmillan, P.N. Brennan, S.J. Forbes, Cell therapy for advanced liver diseases: repair or rebuild, J. Hepatol. 74 (2021) 185–199, https://doi.org/10.1016/j.jhep.2020.09.014.
[31] H.-J. Lee, M.J. Son, J. Ahn, S.J. Oh, M. Lee, A. Kim, Y.-J. Jeung, H.-G. Kim, M. Won, J.H. Lim, N.-S. Kim, C.-R. Jung, K.-S. Chung, Elasticity-based development of functionally enhanced multicellular 3D liver encapsulated in hybrid hydrogel, Acta Biomater. 64 (2017) 67–79, https://doi.org/10.1016/j.actbio.2017.09.041.
[32] M. Cuvellier, F. Ezan, H. Oliveira, S. Rose, J.-C. Fricain, S. Langouët, V. Legagneux, G. Baffet, 3D culture of HepaRG cells in GelMa and its application to bioprinting of a multicellular hepatic model, Biomaterials 269 (2021), 120611, https://doi.org/10.1016/j.biomaterials.2020.120611.
[33] R. Glicklis, J.C. Merchuk, S. Cohen, Modeling mass transfer in hepatocyte spheroids via cell viability, spheroid size, and hepatocellular functions, Biotechnol. Bioeng. 86 (2004) 672–680, https://doi.org/10.1002/bit.20086.
[34] T. Anada, J. Fukuda, Y. Sai, O. Suzuki, An oxygen-permeable spheroid culture system for the prevention of central hypoxia and necrosis of spheroids, Biomaterials 33 (2012) 8430–8441, https://doi.org/10.1016/j.biomaterials.2012.08.040.
[35] D. Mueller, L. Krämer, E. Hoffmann, S. Klein, F. Noor, 3D organotypic HepaRG cultures as in vitro model for acute and repeated dose toxicity studies, Toxicol. Vitro Int. J. Publ. Assoc. BIBRA. 28 (2014) 104–112, https://doi.org/10.1016/j.tiv.2013.06.024.
[36] B.M. Hopkinson, C. Desler, M. Kalisz, P.S. Vestentoft, L. Juel Rasmussen, H.C. Bisgaard, Bioenergetic changes during differentiation of human embryonic stem cells along the hepatic lineage, Oxid. Med. Cell. Longev. (2017), 5080128, https://doi.org/10.1155/2017/5080128, 2017.
[37] S. Tunçer, R. Gurbanov, I. Sheraj, E. Solel, O. Esenturk, S. Banerjee, Low dose dimethyl sulfoxide driven gross molecular changes have the potential to interfere with various cellular processes, Sci. Rep. 8 (2018), 14828, https://doi.org/10.1038/s41598-018-33234-z.
[38] C.K.J. Young, M.J. Young, Comparison of HepaRG cells following growth in proliferative and differentiated culture conditions reveals distinct bioenergetic profiles, Cell Cycle 18 (2019) 476–499, https://doi.org/10.1080/15384101.2019.1578133.
[39] V. Natarajan, E.J. Berglund, D.X. Chen, S. Kidambi, Substrate stiffness regulates primary hepatocyte functions, RSC Adv. 5 (2015) 80956–80966, https://doi.org/10.1039/C5RA15208A.
[40] W. Li, P. Li, N. Li, Y. Du, S. Lü, D. Elad, M. Long, Matrix stiffness and shear stresses modulate hepatocyte functions in a fibrotic liver sinusoidal model, Am. J. Physiol. Gastrointest. Liver Physiol. 320 (2021) G272, https://doi.org/10.1152/ajpgi.00379.2019. –G282.

[41] M. Brovold, D. Keller, M. Devarasetty, A. Dominijanni, R. Shirwaiker, S. Soker, Biofabricated 3D in vitro model of fibrosis-induced abnormal hepatoblast/biliary progenitors' expansion of the developing liver, Bioeng. Transl. Med. 6 (2021), e10207, https://doi.org/10.1002/btm2.10207.
[42] G. Sorrentino, S. Rezakhani, E. Yildiz, S. Nuciforo, M.H. Heim, M.P. Lutolf, K. Schoonjans, Mechano-modulatory synthetic niches for liver organoid derivation, Nat. Commun. 11 (2020) 3416, https://doi.org/10.1038/s41467-020-17161-0.
[43] S. Marchesseau, T. Heimann, S. Chatelin, R. Willinger, H. Delingette, Fast porous visco-hyperelastic soft tissue model for surgery simulation: application to liver surgery, Prog. Biophys. Mol. Biol. 103 (2010) 185–196, https://doi.org/10.1016/j.pbiomolbio.2010.09.005.
[44] D.W. Evans, E.C. Moran, P.M. Baptista, S. Soker, J.L. Sparks, Scale-dependent mechanical properties of native and decellularized liver tissue, Biomech. Model. Mechanobiol. 12 (2013) 569–580, https://doi.org/10.1007/s10237-012-0426-3.
[45] L. Li, A. Maccabi, A. Abiri, Y.-Y. Juo, W. Zhang, Y.-J. Chang, G.N. Saddik, L. Jin, W.S. Grundfest, E.P. Dutson, J.D. Eldredge, P. Benharash, R.N. Candler, Characterization of perfused and sectioned liver tissue in a full indentation cycle using a visco-hyperelastic model, J. Mech. Behav. Biomed. Mater. 90 (2019) 591–603, https://doi.org/10.1016/j.jmbbm.2018.11.006.
[46] D.B. MacManus, M. Maillet, S. O'Gorman, B. Pierrat, J.G. Murphy, M.D. Gilchrist, Sex- and age-specific mechanical properties of liver tissue under dynamic loading conditions, J. Mech. Behav. Biomed. Mater. 99 (2019) 240–246, https://doi.org/10.1016/j.jmbbm.2019.07.028.
[47] I.M. Arias, H.J. Alter, J.L. Boyer, D.E. Cohen, D.A. Shafritz, S.S. Thorgeirsson, A.W. Wolkoff, The Liver: Biology and Pathobiology, sixth ed., Wiley, 2020.
[48] R.P. Tonge, E.J. Kelly, S.A. Bruschi, T. Kalhorn, D.L. Eaton, D.W. Nebert, S.D. Nelson, Role of CYP1A2 in the hepatotoxicity of acetaminophen: investigations using Cyp1a2 null mice, Toxicol. Appl. Pharmacol. 153 (1998) 102–108, https://doi.org/10.1006/taap.1998.8543.
[49] S.B. Jensen, S. Thodberg, S. Parween, M.E. Moses, C.C. Hansen, J. Thomsen, M.B. Sletfjerding, C. Knudsen, R. Del Giudice, P.M. Lund, P.R. Castaño, Y.G. Bustamante, M.N.R. Velazquez, F.S. Jørgensen, A.V. Pandey, T. Laursen, B.L. Møller, N.S. Hatzakis, Biased cytochrome P450-mediated metabolism via small-molecule ligands binding P450 oxidoreductase, Nat. Commun. 12 (2021) 2260, https://doi.org/10.1038/s41467-021-22562-w.
[50] H. Al-Attrache, A. Sharanek, A. Burban, M. Burbank, T. Gicquel, Z. Abdel-Razzak, C. Guguen-Guillouzo, I. Morel, A. Guillouzo, Differential sensitivity of metabolically competent and non-competent HepaRG cells to apoptosis induced by diclofenac combined or not with TNF-α, Toxicol. Lett. 258 (2016) 71–86, https://doi.org/10.1016/j.toxlet.2016.06.008.
[51] C. Aninat, A. Piton, D. Glaise, T. Le Charpentier, S. Langouët, F. Morel, C. Guguen-Guillouzo, A. Guillouzo, Expression of cytochromes P450, conjugating enzymes and nuclear receptors in human hepatoma HepaRG cells, Drug Metab. Dispos. Biol. Fate Chem. 34 (2006) 75–83, https://doi.org/10.1124/dmd.105.006759.
[52] S. Rose, M. Cuvellier, F. Ezan, J. Carteret, A. Bruyère, V. Legagneux, F. Nesslany, G. Baffet, S. Langouët, DMSO-free highly differentiated HepaRG spheroids for chronic toxicity, liver functions and genotoxicity studies, Arch. Toxicol. 96 (2022) 243–258, https://doi.org/10.1007/s00204-021-03178-x.
[53] Z.-Y. Wang, W.-J. Li, Q.-G. Li, H.-S. Jing, T.-J. Yuan, G.-B. Fu, D. Tang, H.-D. Zhang, H.-X. Yan, B. Zhai, A DMSO-free hepatocyte maturation medium accelerates hepatic differentiation of HepaRG cells in vitro, Biomed. Pharmacother. 116 (2019), 109010, https://doi.org/10.1016/j.biopha.2019.109010.
[54] S.B. Leite, I. Wilk-Zasadna, J.M. Zaldivar, E. Airola, M.A. Reis-Fernandes, M. Mennecozzi, C. Guguen-Guillouzo, C. Chesne, C. Guillou, P.M. Alves, S. Coecke, Three-dimensional HepaRG model as an attractive tool for toxicity testing, Toxicol. Sci. 130 (2012) 106–116, https://doi.org/10.1093/toxsci/kfs232.
[55] J.M. Segal, D. Kent, D.J. Wesche, S.S. Ng, M. Serra, B. Oulès, G. Kar, G. Emerton, S.J.I. Blackford, S. Darmanis, R. Miquel, T.V. Luong, R. Yamamoto, A. Bonham, W. Jassem, N. Heaton, A. Vigilante, A. King, R. Sancho, S. Teichmann, S.R. Quake, H. Nakauchi, S.T. Rashid, Single cell analysis of human foetal liver captures the transcriptional profile of hepatobiliary hybrid progenitors, Nat. Commun. 10 (2019) 3350, https://doi.org/10.1038/s41467-019-11266-x.
[56] W.-Y. Lu, T.G. Bird, L. Boulter, A. Tsuchiya, A.M. Cole, T. Hay, R.V. Guest, D. Wojtacha, T.Y. Man, A. Mackinnon, R.A. Ridgway, T. Kendall, M.J. Williams, T. Jamieson, A. Raven, D.C. Hay, J.P. Iredale, A.R. Clarke, O.J. Sansom, S.J. Forbes, Hepatic progenitor cells of biliary origin with liver repopulation capacity, Nat. Cell Biol. 17 (2015) 971–983, https://doi.org/10.1038/ncb3203.
[57] N. Tsukada, C.A. Ackerley, M.J. Phillips, The structure and organization of the bile canalicular cytoskeleton with special reference to actin and actin-binding proteins, Hepatol. Baltim. Md 21 (1995) 1106–1113.
[58] M. Boul, N. Benzoubir, A. Messina, R. Ghasemi, I.B. Mosbah, J.-C. Duclos-Vallée, A. Dubart-Kupperschmitt, B. Le Pioufle, A versatile microfluidic tool for the 3D culture of HepaRG cells seeded at various stages of differentiation, Sci. Rep. 11 (2021), 14075, https://doi.org/10.1038/s41598-021-92011-7.
[59] P. Gissen, I.M. Arias, Structural and functional hepatocyte polarity and liver disease, J. Hepatol. 63 (2015) 1023–1037, https://doi.org/10.1016/j.jhep.2015.06.015.
[60] S. Rose, F. Ezan, M. Cuvellier, A. Bruyère, V. Legagneux, S. Langouët, G. Baffet, Generation of proliferating human adult hepatocytes using optimized 3D culture conditions, Sci. Rep. 11 (2021) 515, https://doi.org/10.1038/s41598-020-80019-4.
[61] N. Tanimizu, N. Ichinohe, Y. Sasaki, T. Itoh, R. Sudo, T. Yamaguchi, T. Katsuda, T. Ninomiya, T. Tokino, T. Ochiya, A. Miyajima, T. Mitaka, Generation of functional liver organoids on combining hepatocytes and cholangiocytes with hepatobiliary connections ex vivo, Nat. Commun. 12 (2021) 3390, https://doi.org/10.1038/s41467-021-23575-1.
[62] Z. Othman, B. Cillero Pastor, S. van Rijt, P. Habibovic, Understanding interactions between biomaterials and biological systems using proteomics, Biomaterials 167 (2018) 191–204, https://doi.org/10.1016/j.biomaterials.2018.03.020.
[63] L.P. Frazão, J. Vieira de Castro, N.M. Neves, In Vivo evaluation of the biocompatibility of biomaterial device, Adv. Exp. Med. Biol. 1250 (2020) 109–124, https://doi.org/10.1007/978-981-15-3262-7_8.
[64] Y. Chen, S. Qiu, Z. He, F. Yan, R. Li, Y. Feng, Comparative analysis of indentation and magnetic resonance elastography for measuring viscoelastic properties, Acta Mech. Sin. 37 (2021) 527–536, https://doi.org/10.1007/s10409-020-01042-2.
[65] E. Fitzpatrick, R.R. Mitry, A. Dhawan, Human hepatocyte transplantation: state of the art, J. Intern. Med. 266 (2009) 339–357, https://doi.org/10.1111/j.1365-2796.2009.02152.x.
[66] T. Tricot, J. De Boeck, C. Verfaillie, Alternative cell sources for liver parenchyma repopulation: where do we stand? Cells 9 (2020) 566, https://doi.org/10.3390/cells9030566.
[67] W.S. Fagg, N. Liu, M.-J. Yang, K. Cheng, E. Chung, J.-S. Kim, G. Wu, J. Fair, Magnetic targeting of stem cell derivatives enhances hepatic engraftment into structurally normal liver, Cell Transplant. 26 (2017) 1868–1877, https://doi.org/10.1177/0963689717737320.
[68] A. Weber, M.-T. Groyer-Picard, D. Franco, I. Dagher, Hepatocyte transplantation in animal models, Liver Transplant. Off. Publ. Am. Assoc. Study Liver Dis. Int. Liver Transplant. Soc. 15 (2009) 7–14, https://doi.org/10.1002/lt.21670.
[69] M. Liu, J. Yang, W. Hu, S. Zhang, Y. Wang, Superior performance of co-cultured mesenchymal stem cells and hepatocytes in poly(lactic acid-glycolic acid) scaffolds for the treatment of acute liver failure, Biomed. Mater. Bristol Engl. 11 (2016), 015008, https://doi.org/10.1088/1748-6041/11/1/015008.
[70] T. Takebe, K. Sekine, M. Enomura, H. Koike, M. Kimura, T. Ogaeri, R.-R. Zhang, Y. Ueno, Y.-W. Zheng, N. Koike, S. Aoyama, Y. Adachi, H. Taniguchi, Vascularized and functional human liver from an iPSC-derived organ bud transplant, Nature 499 (2013) 481–484, https://doi.org/10.1038/nature12271.
[71] L.J. Nelson, M. Navarro, P. Treskes, K. Samuel, O. Tura-Ceide, S.D. Morley, P.C. Hayes, J.N. Plevris, Acetaminophen cytotoxicity is ameliorated in a human liver organotypic co-culture model, Sci. Rep. 5 (2015), 17455, https://doi.org/10.1038/srep17455.
[72] G. Pettinato, S. Lehoux, R. Ramanathan, M.M. Salem, L.-X. He, O. Muse, R. Flaumenhaft, M.T. Thompson, E.A. Rouse, R.D. Cummings, X. Wen, R.A. Fisher, Generation of fully functional hepatocyte-like organoids from human induced pluripotent stem cells mixed with Endothelial Cells, Sci. Rep. 9 (2019) 8920, https://doi.org/10.1038/s41598-019-45514-3.
[73] C. Du, K. Narayanan, M.F. Leong, A.C.A. Wan, Induced pluripotent stem cell-derived hepatocytes and endothelial cells in multi-component hydrogel fibers for liver tissue engineering, Biomaterials 35 (2014) 6006–6014, https://doi.org/10.1016/j.biomaterials.2014.04.011.
[74] J.C. Mossanen, F. Tacke, Acetaminophen-induced acute liver injury in mice, Lab. Anim. 49 (2015) 30–36, https://doi.org/10.1177/0023677215570992.
[75] L. Tolosa, J. Caron, Z. Hannoun, M. Antoni, S. López, D. Burks, J.V. Castell, A. Weber, M.-J. Gomez-Lechon, A. Dubart-Kupperschmitt, Transplantation of hESC-derived hepatocytes protects mice from liver injury, Stem Cell Res. Ther. 6 (2015) 246, https://doi.org/10.1186/s13287-015-0227-6.
[76] K. Taguchi, M. Tokuno, K. Yamasaki, D. Kadowaki, H. Seo, M. Otagiri, Establishment of a model of acetaminophen-induced hepatotoxicity in different weekly-aged ICR mice, Lab. Anim. 49 (2015) 294–301, https://doi.org/10.1177/0023677215573041.
[77] S.S. Ayoub, R.M. Botting, S. Goorha, P.R. Colville-Nash, D.A. Willoughby, L.R. Ballou, Acetaminophen-induced hypothermia in mice is mediated by a prostaglandin endoperoxide synthase 1 gene-derived protein, Proc. Natl. Acad. Sci. USA 101 (2004) 11165–11169, https://doi.org/10.1073/pnas.0404185101.
[78] S. Jitraruch, A. Dhawan, R.D. Hughes, C. Filippi, D. Soong, C. Philippeos, S.C. Lehec, N.D. Heaton, M.S. Longhi, R.R. Mitry, Alginate microencapsulated hepatocytes optimised for transplantation in acute liver failure, PLoS One 9 (2014), e113609, https://doi.org/10.1371/journal.pone.0113609.
[79] C. Zhong, H.-Y. Xie, L. Zhou, X. Xu, S.-S. Zheng, Human hepatocytes loaded in 3D bioprinting generate mini-liver, Hepatobiliary Pancreat. Dis. Int. HBPD INT. 15 (2016) 512–518, https://doi.org/10.1016/s1499-3872(16)60119-4.
[80] H. Yang, L. Sun, Y. Pang, D. Hu, H. Xu, S. Mao, W. Peng, Y. Wang, Y. Xu, Y.-C. Zheng, S. Du, H. Zhao, T. Chi, X. Lu, X. Sang, S. Zhong, X. Wang, H. Zhang, P. Huang, W. Sun, Y. Mao, Three-dimensional bioprinted hepatorganoids prolong survival of mice with liver failure, Gut 70 (2021) 567–574, https://doi.org/10.1136/gutjnl-2019-319960.
[81] H. Rashidi, N.-T. Luu, S.M. Alwahsh, M. Ginai, S. Alhaque, H. Dong, R.A. Tomaz, B. Vernay, V. Vigneswara, J.M. Hallett, A. Chandrashekran, A. Dhawan, L. Vallier, M. Bradley, A. Callanan, S.J. Forbes, P.N. Newsome, D.C. Hay, 3D human liver tissue from pluripotent stem cells displays stable phenotype in vitro and supports compromised liver function in vivo, Arch. Toxicol. 92 (2018) 3117–3129, https://doi.org/10.1007/s00204-018-2280-2.
[82] Y.C. Wu, G.X. Wu, K.W. Chen, L.-Y. Shiu, S. Kumar, G.-S. Liu, S.M. Kuo, Transplantation of 3D adipose-derived stem cell/hepatocyte spheroids alleviates chronic hepatic damage in a rat model of thioacetamide-induced liver cirrhosis, Sci. Rep. 12 (2022) 1227, https://doi.org/10.1038/s41598-022-05174-2.